

State-of-Charge Estimation of Lithium-ion Battery Based on Capacity Degradation Model Considering the Dynamic Currents and Temperatures

Yuan Gao^{1,*}, Rongjie Huang², Dongchen Qin¹, Tingting Wang¹, Shibang Ma³, Shuai Qin¹

¹ School of Mechanical and Power Engineering, Zhengzhou University, Zhengzhou 450001, China

² College of Mechanical and Electrical Engineering, Zhengzhou University of Light Industry, Zhengzhou 450001, China

³ College of Mechanical and Electrical Engineering, Nanyang Normal University, Nanyang 473061, China

*E-mail: im.plateau@qq.com

Received: 10 December 2020 / Accepted: 30 January 2021 / Published: 28 February 2021

The current and temperature are two important factors that influence the performance of lithium-ion batteries. An improved battery model considering dynamic currents and various temperatures is proposed and then applied to battery modeling and state-of-charge (SOC) estimation. A novel capacity model is also employed to reflect real-time capacity degradation. The battery parameter dependencies on current, temperature, and SOC are constructed with a novel semi-empirical approach that combines hundreds of data points obtained from enhanced multiple hybrid pulse power characterization (EMHPPC) tests with the derivation of the Arrhenius equation and the Current-overpotential equation. Finally, the proposed model integrating the unscented Kalman filter (UKF) is employed to estimate the battery SOC. The verification results indicate that the improved method can significantly improve the accuracy of both battery modeling and SOC estimation for broad ranges of current rates and temperatures.

Keywords: Lithium-ion battery; State-of charge; Capacity degradation; Current dependency; Unscented Kalman filter; Electric vehicles.

1. INTRODUCTION

The popularity of fuel vehicles has aggravated global energy shortages and environmental pollution problems [1]. Electric vehicles (EVs) have attracted worldwide attention for their clean, environmentally friendly advantages. Excellent energy density and cycle life make lithium batteries the main or auxiliary power source that is widely used in EVs [2-4]. Establishing an accurate and stable battery model and state estimation algorithm is a fundamental requirement for guaranteeing the safe

and effective operation of batteries. However, there are still some challenging problems. For example, the driving conditions of EVs are complex and changeable. The battery discharge rate can even reach more than 5C in some passing or climbing situations [5]. The ambient temperature of EVs is also not a static value. The temperature in the equatorial region is above 30°C year round, while the temperature in high latitudes can be below 0°C. Under conditions of dynamic current and varying temperature, battery capacity will be degraded, and impedance parameters will also change significantly. This will affect the battery modeling and state estimation.

In recent years, with the rapid development of intelligent algorithms, the mainstream method has been to use on-line parameter estimation methods [6, 7] for battery modeling and state estimation so that the model parameters can be adapted to changes in multiple factors, including the current and temperature [8, 9]. However, there are still many problems in the application of on-line parameter identification. For example, the accuracy of on-line parameter estimation is lower than that of the off-line identification method, but the amount of calculation increases significantly. If the battery current changes dramatically in a short time, the on-line parameter identification method cannot react in time, resulting in an increased simulation error. Moreover, the on-line parameter estimation method is a demand-oriented method [10] that is more concerned with the final output results, such as whether the obtained terminal voltage and SOC meet the requirements rather than whether the battery parameters can accurately follow the changes in temperature and current during the calculation process. It is more fundamental to study the influence of the changeable external environment on the capacity, resistance, and other core parameters of batteries, all of which are of great significance to researchers in their study of the mechanism of batteries, the improvement in battery performance, and the choice of suitable batteries used for EVs [11]. All of the above requirements rely on accurate off-line parameter identification methods rather than the on-line parameter estimation method.

The existing off-line parameter identification methods [12-14] mainly focus on the effect of temperature on battery performance. Lithium-ion batteries exhibit different capacity characteristics, impedance characteristics, and polarization characteristics at different ambient temperatures [14]. It is generally believed that there will be a degraded power performance [15] associated with lower electrolyte conductivity, slower electrochemical reaction rate, and a decrease of the diffusion rate of Li⁺ ions at low temperatures [12]. Several publications [16-18] used the Arrhenius equation to describe the relationship between battery internal resistance, capacity, and temperature and achieved good results. Much of the literature [13, 19, 20] has provided powerful evidence concluding that high accuracy of battery modeling, SOC, and SOH estimation can be obtained when considering temperature dependency. All the above studies can obtain reasonable precision and robustness by using temperature-dependent battery models with small current profiles. However, when those models that ignore the effects of current are applied to the highly dynamic load profiles commonly seen in EVs, significant deviations will be found.

The resistance dependency characteristics and capacity of the battery are also affected by current, but few related studies have been found. Waag [21] observed that the internal resistance of lithium-ion batteries significantly decreases as the current increases, especially at lower temperatures. Zhu [22] found an apparent reduction in the semicircle of the impedance with an increasing current rate using the AC impedance technique at medium-frequencies. The current impedance characteristics

can be mainly attributed to non-linear behavior, which can be described by the Butler-Volmer equation (BVE) [23, 24]. This equation indicates that the charge transfer resistance tends to decrease when the current becomes large. However, it is different to be applied in practical engineering due to the large number of variables to be identified, in addition to the complicated calculations. Ratnakumar [25, 26] simplified the BVE by ignoring the reverse electrochemical reaction at sufficiently high currents to clearly express the linear relationship between the impedance and the reciprocal of the current magnitude of lithium-ion batteries used in Mars Exploration Rovers. However, unacceptable errors were obtained when this simplified equation is applied to the batteries for EVs, such as LFP batteries and NMC batteries. Fleischer [27] and Zhu [28] retained the strong current term of the BVE and achieved certain accuracy in lithium-ion batteries for EVs by assuming the same chemical reaction rates at the anode and cathode and treating the active substance concentration at the interface and electrode as a fixed value during the entire charge-discharge process. However, that ideal state does not exist. There is a deviation in the reaction rates at the anode and cathode, and the concentration of oxidants and reductants, both at the interface and electrode, vary dynamically under different currents, temperatures, and SOC. Moreover, when jointly considering the influence of current, temperature, and SOC on the battery parameters, neither the Arrhenius equation nor the BVE can meet the requirements well, so the parameter identification method must be further improved.

The primary purpose of studying the factors affecting battery performance is to apply them to battery modeling and state estimation. Due to the importance of the SOC in battery management system (BMS), SOC estimation methods have become a hot field in recent years. Several on-line SOC estimation methods, such as machine learning method [29] and model-based method have been developed by researchers, replacing the previous ampere-hour integration method and open circuit voltage (OCV) method. With the development of advanced algorithms and the improvement of computing performance, the use of machine learning methods has achieved vigorous application. neural network [30], support vector mechanism [31], genetic algorithm [32] and other mechanical learning methods are used for SOC estimation. The calculation processes of these machine learning methods is similar. They all take a large amount of battery test data as input and process them in the middle layer to establish the relationship between input and output, and finally output the needed parameters, such as SOC. It is especially suitable in the simulation of highly non-linear battery systems by optimizing a large amount of data to minimize errors. However, the machine learning method requires a large amount of original data in the process of adapting to learning, and the entire training process is long. Compared with machine learning methods, model-based methods also result in good accuracy, but the amount of calculation is great reduced, making it more suitable for EV applications.

Several model-based methods for SOC estimation have been developed, such as the particle filter algorithm [33, 34], H_{∞} filter [35-37], and a series of improved Kalman filters [38-41]. These filter techniques use the observation equation of the terminal voltage to correct the initial SOC guess and reduce the accumulated error to obtain better robustness. The core work of the model-based method is to select suitable battery models and algorithm tools [42, 43]. Choosing an appropriate battery model can improve the accuracy of the state equation and observation equation, and an appropriate algorithm tool is critical to the efficiency of the model-based method. There are many

studies of algorithm tools, such as AEKF [44], SRUKF [45], and CKF [46]; however, the battery model they use is often relatively simple. As analyzed above, current and temperature will cause battery capacity degradation and the changes in battery parameters, thereby affecting the output of the battery. Therefore, when an advanced algorithm tool is employed for SOC estimation, considering the impact of dynamic currents and temperatures on the battery will improve its accuracy [9, 47, 48].

An accurate battery model is a prerequisite to ensure the accuracy of the model-based method. Various kinds of battery models have been proposed in recent decades, such as the equivalent circuit model (ECM) [49], electrochemical models [50, 51], and neural network models [52, 53]. Electrochemical model and neural network model are less common in engineering applications because of their complex structure and excessive training data, respectively. However, due to its convenient calculation and good accuracy, ECM is widely used in EVs [54, 55]. Some scholars [20] have increased the number of resistance-capacitance (RC) networks to better express the polarization effect of lithium-ion batteries or have regarded the ECM parameters as a function of temperature and SOC to improve the modeling accuracy. In addition, battery parameters are also affected by the current, and the current fluctuates significantly in the actual driving of EVs. However, only a few scholars have considered the influence of current when modeling batteries. These studies are all based on the approximation of the BVE, and the research that applies the current dependency model to state estimation is even rarer [21-23]. As far as we know, there is no literature concurrently considering the effects of current and temperature at the same time for battery modeling and integrating the closed-loop filtering method for on-line SOC estimation.

The motivation of this work is to develop a novel and efficient capacity and battery parameter identification approach for ensuring the accuracy of the battery model and SOC estimation under dynamic conditions. The contributions of this article include 1) a second-order ECM is developed considering the dependency of the parameters not only on temperature and SOC but also on current; 2) an real-time capacity degradation model (RCDM) is proposed to calculate the actual capacity under dynamic currents and temperatures; and 3) a novel semi-empirical approach for parameters identification based on the transformation of the Arrhenius equation and Current-overpotential equation is proposed. To illustrate the applicability of the model, the improved model integrating the unscented Kalman filter (UKF) algorithm is extended and applied to SOC estimation. With the above contributions, our study can enable easier availability of accurate values of actual capacity and parameters for advanced battery management. Verification test results show that the proposed model can better express the voltage response in battery modeling and achieve better accuracy in SOC estimation.

2. BATTERY MODEL

2.1 ECM with current dependency, temperature dependency, and SOC dependency

The ECM uses a network of electrical elements such as voltage sources, resistors, and capacitors to simulate the current-voltage dynamic behaviors of the battery. With the advantage of

simplicity and high accuracy in characterizing the transient response and polarization effect of batteries, it is frequently applied in research and engineering [55]. Usually, ECM only contains one RC network, and the resistances and capacitances of the ECM are parameterized as a function of temperature and battery SOC. We construct an improved ECM, as shown in Figure 1, with a second-order RC network, and the battery parameters are jointly affected by current, temperature, and SOC to more realistically represent the variable electrical behaviors of the battery used in EVs under complex driving conditions.

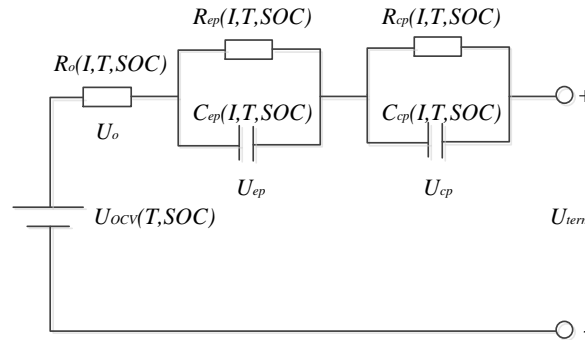


Figure 1. The equivalent circuit model.

In Figure 1, R_o is the ohmic resistance, which is produced by the active material, electrolyte, and conductance of contacts. R_{ep} and C_{ep} are the electrochemical polarization resistance and capacitance, respectively, and R_{cp} and C_{cp} are the concentration polarization resistance and capacitance, respectively. All the resistances and capacitances depend on the battery SOC, temperature, and current. U_{OCV} is the OCV that depends on the battery SOC and temperature, U_o is the terminal voltage of R_o , U_{ep} and U_{cp} are the voltages of the 2RC networks, and U_{term} is the terminal voltage of the battery. I is the load current with a positive value in the discharging process and a negative value in the charging process.

The improved ECM conforms to Kirchhoff's laws, and we can obtain:

$$U_{term} = U_{ocv}(T, SOC) + U_o + U_{ep} + U_{cp} \quad (1)$$

$$U_o = IR_o(I, T, SOC) \quad (2)$$

$$\frac{dU_{ep}}{dt} + \frac{U_{ep}}{R_{ep}(I, T, SOC)C_{ep}(I, T, SOC)} = \frac{I}{C_{ep}(I, T, SOC)} \quad (3)$$

$$\frac{dU_{cp}}{dt} + \frac{U_{cp}}{R_{cp}(I, T, SOC)C_{cp}(I, T, SOC)} = \frac{I}{C_{cp}(I, T, SOC)} \quad (4)$$

U_{OCV} can be obtained by an OCV–SOC–T table [56], which is commonly used in battery modeling. The identification method of the parameters (R_o , R_{ep} , R_{cp} , C_{ep} , and C_{cp}) involved in the ECM will be elucidated in Section 3, and the SOC estimation algorithm will be introduced in Section 4.

2.2 Real-time capacity degradation model

Capacity is one of the essential indicators to measure battery performance and is also the basis of SOC estimation. The nominal capacity refers to the discharged electricity amount tested by the battery manufacturer under specific conditions. However, the driving environment of EVs and the driving habits of users are variable, thus there is a large difference between these and the battery manufacturer test conditions. Therefore, the actual capacity of the battery has a particular difference from the nominal capacity. For example, the actual capacity has a significant degradation at subzero temperatures and can be decreased to only 30% of the nominal capacity at -25°C. The actual battery capacity is also different under different numbers of cycles [57]. Usually, a polynomial function formulated by fitting the experimental data is employed to address the relationship between actual capacity and temperature as:

$$C_{ac}(T) = aT^3 + bT^2 + cT + d \tag{5}$$

The capacity is an important input variable of the state equation for battery SOC estimation. Real-time tracking of battery capacity is the key to ensuring the accuracy of SOC estimation. Most of the existing research [13] only pays attention to the influence of temperature on the actual capacity of the batteries. They adopts equation (5) to express the change of capacity during operation, however, the actual capacity is also affected by the current. The tested capacity under different temperatures and currents is shown in Figure 2. The battery's actual capacity decreases significantly with increasing discharge current rate when the temperature is below 25°C, and the quantity of electric charge discharged with a 3 C constant current is 93.2% of that with a 0.1C current at 5°C.

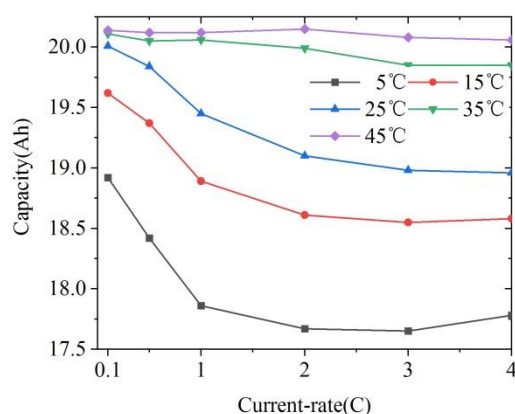


Figure 2. Tested battery capacity under different temperature and current.

However, there is little literature that can accurately reveal the dependency of actual capacity on current. Moreover, it is also inappropriate to express that relationship by simply using a polynomial or current correction factor obtained by fitting the total released capacity under different discharge currents. Because the actual capacity obtained at this time is the final accumulation result of the entire constant current discharge process, the loading current in EVs is not a constant and will change drastically in a short time during acceleration, climbing, or braking. That final accumulation result

cannot be used to represent the actual battery capacity at a certain current moment under dynamic loading. To establish a RCD model, a novel concept called the capacity degradation rate $dC(I, T)$ is proposed to reflect the dynamic changes in battery capacity at each discharge instant. It is a function of current and temperature and can be described as:

$$dC(I, T) = \frac{C_{\max}(T) - C_{\text{fin}}(I, T)}{t_d(I)} \tag{6}$$

where $C_{\max}(T)$ is the maximum capacity that the battery can release at temperature T . Since the battery can be discharged more fully with a small current, $C_{\max}(T)$ is approximately equal to the actual capacity released with a 0.1C current-rate. $C_{\text{fin}}(I, T)$ is the final released capacity with current I at temperature T . $Td(I)$ is the required time of battery discharge to the cut-off voltage with a constant current I . $t_d(I)$ is 3600 s with a 1C discharge current and 1800 s with a 2C discharge current.

$C_{\max}(T)$ and $C_{de}(t)$ can be formulated by fitting the experimental data as in equation (3) and equation (4).

$$C_{\max}(T) = 2.83e - 5T^3 - 3.43e - 3T^2 + 0.145T + 18.2 \tag{7}$$

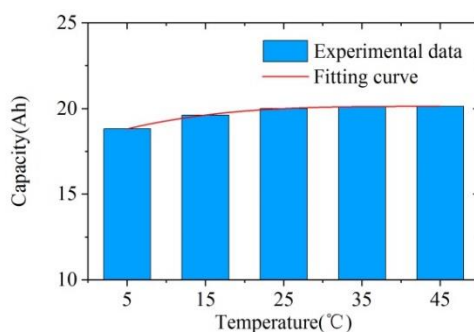


Figure 3. Relationship between capacity and temperature.

$$dC(I, T) = 2.18e - 5\left(\frac{I}{20}\right)^3 - 0.00162\left(\frac{I}{20}\right)^2 + 0.03398\left(\frac{I}{20}\right) - 0.01453T^3 + 0.09312T^2 + 0.1952T - 0.0001692\left(\frac{I}{20}\right)^2T - 0.195 \tag{8}$$

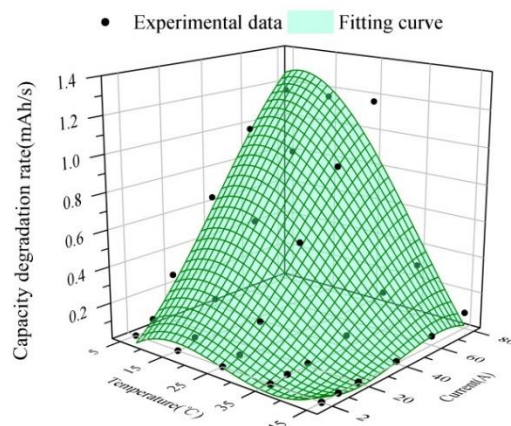


Figure 4. Capacity degradation rate.

$dC(I, T)$ is a measure of the sensitivity of the current to battery capacity degradation, and the unit of $dC(I, T)$ is mAh/s. The difference between $C_{max}(T)$ and $C_{fin}(I, T)$ represents the total degradation capacity after the battery is fully discharged with current I . Then, the quotient of the total degradation capacity and total discharge time is the degradation capacity caused by the current I at each time point. Therefore, the total degradation capacity can be obtained by integrating the capacity degradation rate as:

$$C_{de}(t) = \int_0^t dC(I, T) dt \tag{9}$$

Finally, the RCDM under dynamic current conditions is calculated by subtracting the total degradation capacity $C_{de}(t)$ from time 0 to t from the maximum capacity $C_{max}(T)$ that can be released at temperature T .

$$C_{ac}(I, T, t) = C_{max}(T) - C_{de}(t) \tag{10}$$

3. A SEMI-EMPIRICAL APPROACH FOR PARAMETERS IDENTIFICATION

3.1. Battery test bench

The parameter identification tests, and the verification tests performed in section 5 are all carried out on the battery test platform, as shown in Figure 2. The test platform consists of 1) prismatic lithium-ion batteries, and the key specifications are shown in Table 1; 2) a PC with a group of LAND data software for charging/discharging process control and data acquisition, and MATLAB for data analysis; 3) a LAND CT6001A(4CH) battery test system; and 4) a Biolab BLC-300 incubator in which the tested batteries are placed. The sampling cables connect all the above devices, and the sampling time of the current and voltage during the test process is 1 s.

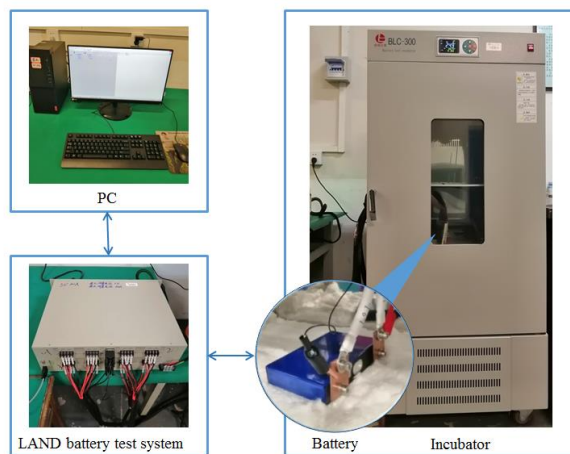


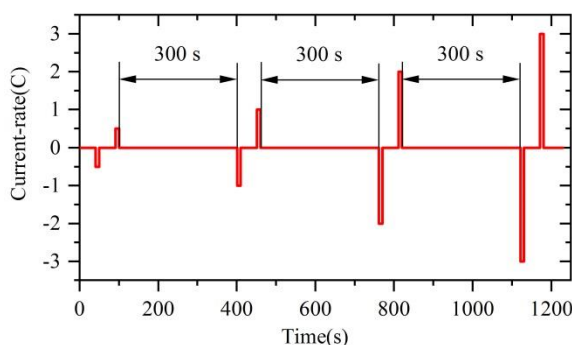
Figure 5. The framework of the battery test bench.

Table 1. The key specifications of the test batteries.

| Type | Nominal voltage | Nominal capacity | Upper cut-off voltage | Lower cut-off voltage | Maximum continuous discharge rate |
|--------------------|-----------------|------------------|-----------------------|-----------------------|-----------------------------------|
| LiFeO ₄ | 3.2V | 20Ah | 3.65V | 2.5V | 5C |

3.2. Empirical approach for parameter identification

HPPC is a relatively effective experimental method to identify battery parameters at tested points. It is composed of a 10 s constant current discharging process and a 10 s constant current charging process with a 40 s interval. Usually, each current pulse must be separated by more than 1 hour to cause the battery to reach the equilibrium state.

**Figure 6.** Current profile of the EMHPPC.

However, hundreds of HPPC tests must be performed when the parameters are used to simultaneously investigate the dependency on current, temperature, and SOC. Meanwhile, the one-hour interval becomes a thorny problem because the total test time increases significantly as the number of tests increases. In fact, the terminal voltage of the battery stabilizes after a 300-second standstill after the HPPC test. At this time, the battery can be approximately in an equilibrium state. Therefore, this paper uses the EMHPPC method to save experiment time, it includes four independent HPPC tests with current-rates of 1/2C, 1C, 2C, and 3C, while the interval between each test is 300 s instead of 3600 s. The current profile of an EMHPPC test cycle is shown in Figure 6.

The model-identification test procedures comprise numerous EMHPPC tests performed at different temperatures (5°C, 15°C, 25°C, 35°C, 45°C). The tested SOC ranges from 100% to 0% with an interval of 10%, and we add two test points at 95% SOC and 5% SOC to improve the accuracy of the identification tests in the high and low ranges of SOC. The measured current, measured voltage, and cumulative SOC at 35°C are shown in Figure 7.

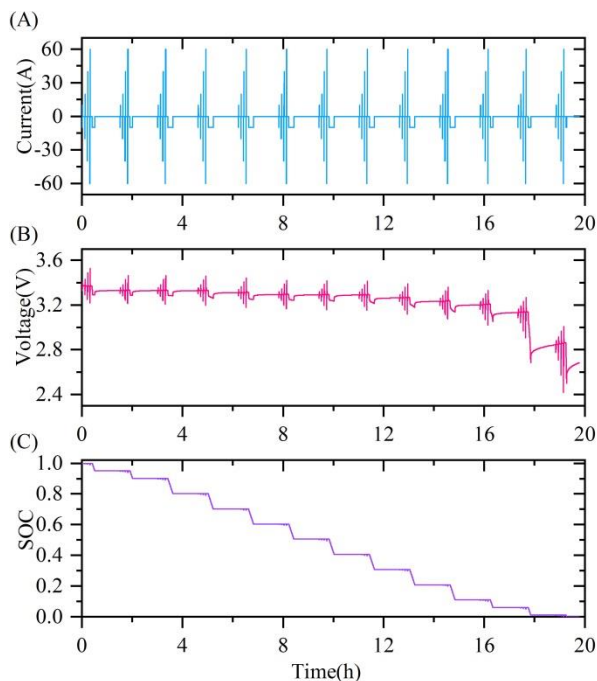


Figure 7. Model-identification test profile at 35°C: (A) current; (B) voltage; (C) SOC.

3.3. Analysis of empirical results and construction of the semi-empirical method

The battery parameters (R_o , R_{ep} , R_{cp} , C_{ep} , and C_{cp}) can be extracted from the EMHPPC test results by employing the Levenberg-Marquard algorithm. However, the utilization of empirical method has limitations. It cannot simulate the changes in battery parameters under all operating conditions with a limited number of test points even though hundreds of EMHPPC tests have been performed.

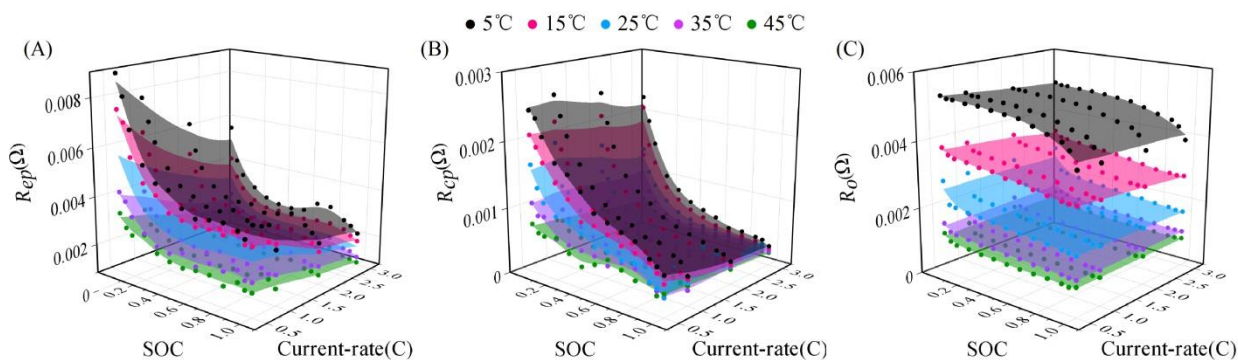


Figure 8. Empirical results (scatters) and resistances identification model (surface plots) of R_o (A), R_{ep} (B), R_{cp} (C) at different current-rates, temperatures, and SOC.

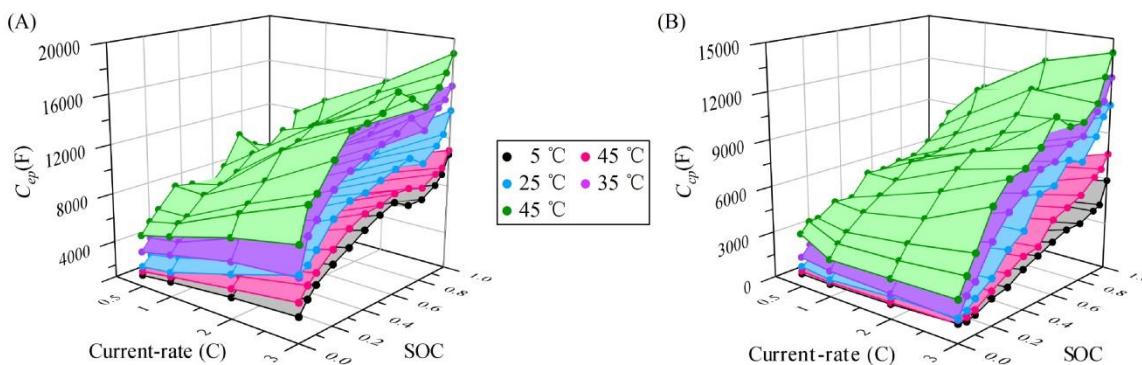


Figure 9. Empirical results (scatters) and capacitances identification model (surface plots) of C_{ep} (A), C_{cp} (B) at different current-rates, temperatures, and SOC.

Therefore, it is necessary to analyze the empirical results, determine the parameter change trends, study the influence mechanism of battery parameters by current, temperature, and SOC, combine the empirical results and electrochemical mechanism, and finally establish a more accurate parameter identification approach. The following section will expand on a thorough analysis and modeling of the dependence of the parameters on current, temperature, and SOC using a semi-empirical method. The resistances and capacitances extracted from the EMHPPC and the semi-empirical approach are given in Figure 8 and Figure 9.

3.3.1. Investigation of the resistances dependency on temperature

All the resistances increase with decreasing temperature in Figure 8, but the change rate of resistances at different temperatures is not the same. When the temperature is high, especially above 35°C, the resistances increase slightly with the temperature; by contrast, the resistances increase significantly when the temperature is below 15°C. This is because the resistance is closely related to the diffusion rate of Li^+ ions [58]. Several publications [16-18] have indicated that the resistance is closely associated with the diffusion rate of Li^+ ions, and the relationship between the diffusion rate of particles and temperature follows the Arrhenius equation. It can be given as:

$$k = A \exp\left(-\frac{Ea}{RT}\right) \tag{11}$$

where k is the reaction rate constant, Ea is the activation energy, R is the Molar gas constant, T is the temperature, and A is the Arrhenius constant.

This equation shows that the reaction rate constant k has an exponential relationship with temperature, so the reaction rate decreases sharply at low temperatures. The battery resistance is positively correlated with the reciprocal of the reaction rate constant ($R = B/k$, where B is a constant). A lower reaction rate means that the particles with greater difficulty and the electrochemical reaction rate of the positive and negative electrodes will be slow. This causes the distribution of Li^+ ions in the electrolyte to become uneven, exacerbating the electrochemical polarization effect and concentration polarization effect. The conductivity of the electrolyte also decreases as the temperature decreases.

Therefore, the resistances R_o , R_{ep} , and R_{cp} all increase with decreasing temperature. Then, the battery resistances can be denoted as:

$$R_o + R_{ep} + R_{cp} = \frac{B}{A} \exp\left(\frac{Ea}{RT}\right) \quad (12)$$

Taking the logarithm of both sides of equation (17), the dependency of the battery resistances on temperature can be more clearly expressed as:

$$\ln(R_o + R_{ep} + R_{cp}) = \frac{Ea}{R} \ln \frac{B}{A} \frac{1}{T} \quad (13)$$

The $\ln(R_o + R_{ep} + R_{cp})$ versus $1/T$ is plotted here, which shows an approximately linear relationship between them. Additionally, Figure 10 indicates that the Arrhenius equation can well describe the relationship between resistance and temperature at different SOC and current-rates.

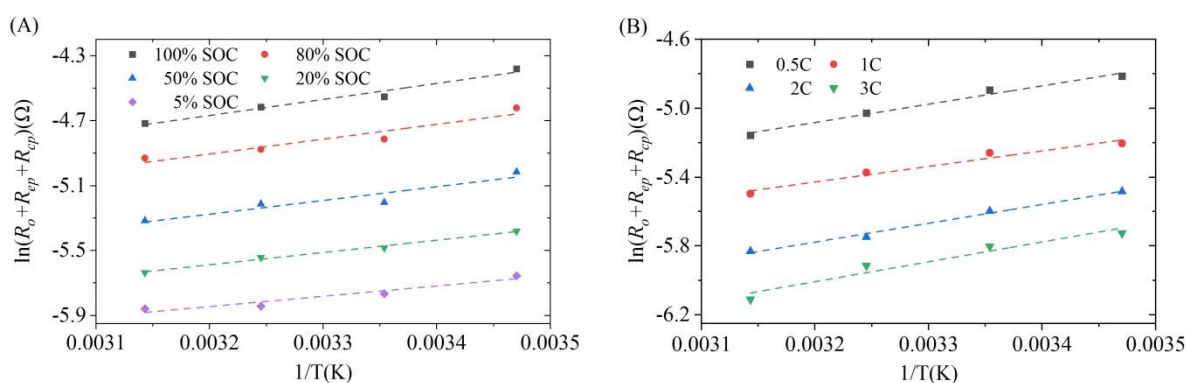


Figure 10. Temperature dependency of battery resistances at 1/2C (A) and 50% SOC (B). The experiment data (scatters), the fitting results (dashed lines).

3.3.2. Investigation of the resistances dependency on current

As shown in Figure 8, the current dependency of the ohm resistance R_o can be neglected. When the temperature is above 5°C, the value of R_o is basically unchanged with different current rates; when the temperature is below 5°C, the resistance R_o slightly decreases as the discharge rate increases, which is mainly due to the relatively noticeable temperature rise caused by the battery at high discharge currents. The electrochemical polarization resistance R_{ep} and the concentration polarization resistance R_{cp} have the same trend affected by the current, and they both decrease with increasing current rate. The mechanism of the current on the battery polarization resistance is mainly attributed to the non-linear behavior of the charge transfer reaction. The Butler-Volmer equation is usually employed to approximate that behavior as:

$$i = i_o \left[\exp\left(\frac{\alpha_a n F}{RT} V_o\right) - \exp\left(-\frac{\alpha_c n F}{RT} V_o\right) \right] \quad (14)$$

Under dynamic current and temperature conditions, the application of BVE has limitations, mainly due to accuracy issues. Therefore, this paper chooses the Current-overpotential equation to express the relationship between the current and charge transfer resistance of lithium-ion batteries. It is a more rigorous description of the laws of electrochemical kinetics. Actually, BVE is just an ideal state

of the Current-overpotential equation by assuming that the concentration of the active material in interface and electrodes is equal. However, that ideal state exists only when the current is small and the solution concentration is absolutely uniform which is quite rare in EVs.

$$i = i_o \left[\frac{C_o}{C_o^*} \exp\left(\frac{\alpha_a nF}{RT} V_o\right) - \frac{C_R}{C_R^*} \exp\left(-\frac{\alpha_c nF}{RT} V_o\right) \right] \quad (15)$$

where A is the electrode active surface area, i is the transfer current, i_o is the exchange current density, C_o and C_o^* are the concentrations in the interface and anode of the oxidants, C_R and C_R^* are the concentrations in the interface and cathode of the reductants, α_a and α_c are the anodic and cathodic transfer coefficients ($\alpha_a + \alpha_c = 1$, $\alpha_a > 0$, $\alpha_c > 0$), n is the number of electrons involved in the charge transfer process, F is the Faraday constant, R is the gas constant, T is the temperature, and V_o is the overpotential.

The inverse of the hyperbolic function $\sinh(x) = 0.5 \cdot [a \cdot \exp(x) - b \cdot \exp(-x)]$ is:

$$\sinh^{-1}(x) = \ln\left(\frac{x + \sqrt{x^2 + ab}}{a}\right) \quad (16)$$

The electrochemical reaction mechanisms at the anode and cathode during the charging and discharging process of lithium batteries are very similar, so the cathode and anode transfer coefficients can be assumed to be equal ($\alpha_a = \alpha_c = 0.5$) [22]. Using the substitutions $\lambda_o = C_o/C_o^*$, $\lambda_R = C_R/C_R^*$, and $K = 1/(2 \cdot A \cdot i_o)$, and according to equation (8), the Butler-Volmer equation can be denoted as:

$$\frac{nF}{2RT} V_o = \ln\left[\frac{Ki + \sqrt{(Ki)^2 + \lambda_o \lambda_R}}{\lambda_o}\right] \quad (17)$$

Then, the charge transfer resistance is defined as:

$$R_{ct} = \frac{V_o}{i} = \frac{2RT}{nFi} \ln\left[\frac{Ki + \sqrt{(Ki)^2 + \lambda_o \lambda_R}}{\lambda_o}\right] \quad (18)$$

For EVs, the transfer internal resistance of a lithium battery is approximately equal to the internal polarization resistance, and the transfer current i is also considered to be approximately equal to the battery terminal current I . Therefore, the relationship between polarization resistances and current can be described as:

$$R_p = \frac{2RT}{nFI} \ln\left[\frac{KI + \sqrt{(KI)^2 + \lambda_o \lambda_R}}{\lambda_o}\right] \quad (19)$$

Some scholars [27] have retained the reverse electrochemical reaction under high current but regarded the concentration ratio of the active material at the reaction interface and the electrode as a fixed value. They have expressed the relationship between the internal polarization resistance of the battery and the current as:

$$R_p = \frac{2RT}{nFI} \ln\left[KI + \sqrt{(KI)^2 + 1}\right] \quad (20)$$

Other researchers [25] believe that the reverse electrochemical reaction can be ignored when the current is sufficiently high because the overpotential V_o is high enough in this case. They regard

the polarization resistance and the reciprocal of the current as having an approximately linear relationship:

$$R_p = k \frac{1}{I} + b \tag{21}$$

where k and b are the fitting constants.

It is worth noting that although regarding the concentration ratio of the active material at the reaction interface and the electrode as a fixed value ($\lambda_O = \lambda_R = 1$) can reduce the calculation of BVE, the error also increases significantly. Equation (20) which is derived from the BVE can no longer accurately reflect the relationship between battery polarization resistance and current. Both the concentration ratio of the active material at the reaction interface and electrode vary from 0 to 1. Although the form of equation (21) is very simple, it ignores too many factors that must be considered, and this approximate linear relationship is not applicable to lithium batteries.

The relationship between the internal polarization resistance and the current obtained in Section 3 is shown in Figure 11. It can be seen from the figure that the proposed equation can better describe the relationship between the polarization internal resistance and current.

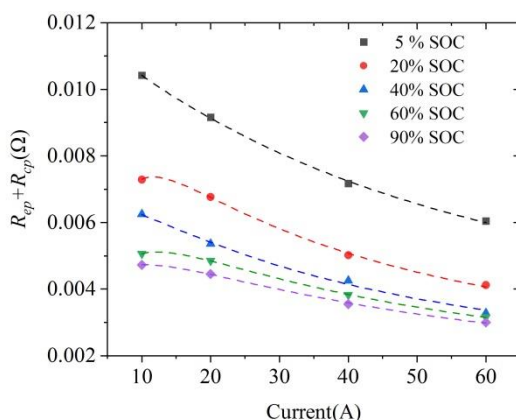


Figure 11. Current dependency of battery polarization resistances. The experiment data (scatters), the fitting results (dashed lines).

3.3.3 Investigation of the parameters dependency on current, temperature, and SOC

Although equation (19) can be used to describe the current dependency on battery polarization resistance, the polarization internal resistance is also affected by temperature. To interpret the coupling relationships between polarization resistance, current, and temperature, equation (22) requires further processing. According to porous electrode theory, the exchange current density i_o is an indicator of the internal electrochemical reaction, which reflects the difficulty of charge moving from the electrolyte to the reaction interface and is analogous to the reaction rate constant k in Arrhenius equation. So i_o [59] can also be described by the Arrhenius equation as:

$$i_o = C \exp\left(-\frac{Ea}{RT}\right) \tag{22}$$

where C is a constant used to express the exponential relationship between exchange current density and temperature.

Following equations (19) and (22) and using the substitutions $a_1^\omega = 2 \cdot R / (n \cdot F)$, $a_2^\omega = 0.5 / (A \cdot C)$, and $a_3^\omega = Ea/R$, the polarization resistance on current and temperature dependency can be given as:

$$R_\omega(I, T) = a_1^\omega \frac{T}{I} \left\{ \ln \left[a_2^\omega \exp\left(\frac{a_3^\omega}{T}\right) I + \sqrt{\left(a_2^\omega \exp\left(\frac{a_3^\omega}{T}\right) I \right)^2 + \lambda_o \lambda_R} \right] - \ln \lambda_o \right\} \quad (23)$$

where $\omega = ep$ for R_{ep} , and $\omega = cp$ for R_{cp} .

SOC is another crucial factor affecting battery impedance. As SOC decreases, active materials in the electrolyte will be reduced, and the conductivity of electrolytes will also decrease, which leads to increased resistance. The resistances have more significant fluctuations when the SOC is below 20%, especially the SOC is nearby 0%. At this time, most of the lithium-ions have been inserted into the positive electrode when the SOC is below 20%, which will lead to the following results: 1) Large amounts of compounds wrapper on the positive electrode so that the contact resistance will increase. 2) Due to the reduction of the active materials, the electrochemical reaction rates of the positive electrode and negative electrode decrease, and the electrochemical polarization becomes more intense. 3) The concentration of lithium-ions at the positive electrode gradually approaches saturation, and it will be more difficult for lithium-ions to diffuse and insert into the positive electrode, which will aggravate the concentration polarization effect. Lower conductivity of the electrolytes and higher contact resistance result in an increase in the ohm resistance R_o ; a more intense electrochemical polarization effect and concentration polarization effect lead to increases in the resistance R_{ep} and R_{cp} .

However, there is no accurate model to describe the relationship between battery resistances and SOC, so this paper employs a polynomial regression to approximate the resistance dependency on SOC. Then, equation (23) can be extended as follows:

$$R_\omega(I, T, SOC) = f_\omega(SOC) R_\omega(I, T) \quad (24)$$

$$f_\omega(SOC) = b_1^\omega SOC^3 + b_2^\omega SOC^2 + b_3^\omega SOC + b_4^\omega \quad (25)$$

Figure 5e indicates that the ohmic resistance is basically unchanged under different currents when the temperature is above 5°C. Then the ohmic resistance dependency on current can be seen as a constant D , and the Arrhenius equation and polynomial function can also be used to express the ohmic resistance dependency on temperature and SOC. Therefore, R_o is calculated by the formula:

$$R_o(I, T, SOC) = g(SOC) h(I) R_o(T) \quad (26)$$

$$R_o(T) = c_1 \exp\left(\frac{c_2}{T}\right) \quad (27)$$

$$g(SOC) = d_1 SOC^4 + d_2 SOC^3 + d_3 SOC^2 + d_4 SOC + d_5 \quad (28)$$

$$h(I) = D \quad (29)$$

where $a_1^\omega \sim a_3^\omega$, $b_1^\omega \sim b_4^\omega$, c_1 , c_2 , $d_1 \sim d_5$, and D are the fitting parameters. It can be concluded that equations (24) and (26) used to calculate the battery resistances can describe the experimental data with high quality as shown in Figure 8.

The battery parameters that must be identified include not only resistances but also capacitances (C_{ep} and C_{cp}). As shown in Figure 9, the capacitance is also affected by the current, temperature, and SOC. Unlike the resistance, the capacitance shows an upward trend with increasing

temperature and current. C_{ep} and C_{cp} fluctuate sharply over the whole SOC range, but overall, the capacitances increase with climbing SOC. However, the current research focuses mainly on battery resistance but less on capacity, and there is no specific mathematical model that can accurately express the complicated relationship between capacitance and current, temperature, and SOC. In this study, the C_{ep} and C_{cp} values at different currents, temperatures, and SOCs are formulated from the empirical results with the piecewise linear interpolation method shown in Figure 9.

4. SOC ESTIMATION METHOD CONSIDERING THE CAPACITY DEGRADATION

SOC estimation of batteries is a typical non-linear problem. There are many existing SOC estimation methods to address non-linear problems, such as particle filter [60], neural network [61] and a series of improved Kalman filter algorithms. All of these methods use advanced algorithms to improve the accuracy of SOC estimation. The final SOC estimation accuracy obtained by those algorithms is similar; however, the differences are in the specific calculation steps and algorithm robustness. The general form of the state space equation of a non-linear system is represented as:

$$x_k = f(x_{k-1}, u_{k-1}) + \omega_{k-1} \quad (30)$$

$$y_k = g(x_k, u_k) + v_k \quad (31)$$

where x_k and y_k are the prediction vector and measurement vector at time k , respectively, ω_{k-1} is the prediction noise, and v_k is the measurement noise, which is subject to a normal distribution, and u_k is the input control vector.

These advanced algorithms are nothing more than tools to improve the existing accuracy or reduce the amount of calculation, and their state equations have not changed substantially. If you want to further improve the accuracy of SOC estimation, you must not only rely on advanced algorithms but also conduct more basic research on the state space equation and battery model. In this paper, the RCDM proposed in Section 2 is used to improve the state space equation for SOC estimation. In addition, based on the study of the influence of current and temperature on impedance introduced in Section 3, a more accurate battery model is established to improve the accuracy of the input vector of the state equation and observation equation. The improved state equation is shown as:

$$SOC_k = SOC_{k-1} - \frac{I_{k-1}}{C_{ac}(I, T, t)} \quad (32)$$

By combining the improved state and observation equation, the UKF algorithm with better accuracy and stability is employed to estimate the SOC. The core idea of UKF [62-64] is to use the unscented transformation to approximate the state distribution of the non-linear system calculation results. UKF selects a minimal set of sampling points, called the sigma points, according to some specific rules to estimate the mean and variance of the Gaussian variable after non-linear processing. UKF has been successfully applied in battery SOC estimation and has achieved good accuracy. The implementation details of the UKF are summarized in Table 2.

Table 2. The specific steps of the UKF algorithm.

Summary of the UKF algorithm

- Algorithm initialization :

Initial states: $\hat{x}_o = E(x_o)$

Initial covariance: $P_o = E[(x_o - \hat{x}_o) \cdot (x_o - \hat{x}_o)^T]$

- Generate Sigma points:

$$x_{k-1}^o = \hat{x}_{k-1}$$

$$x_{k-1}^i = \hat{x}_{k-1} + \left(\sqrt{(n+\lambda)P_{k-1}} \right)_i$$

$$x_{k-1}^{i+n} = \hat{x}_{k-1} - \left(\sqrt{(n+\lambda)P_{k-1}} \right)_i$$

Distribute weights:

$$\omega_m^o = \frac{\lambda}{n+\lambda}$$

$$\omega_c^o = \frac{\lambda}{n+\lambda} + 1 - \alpha^2 + \beta$$

$$\omega_m^i = \omega_c^i = \frac{1}{2(n+\lambda)}$$

- Prediction update:

Update sigma points through prediction function:

$$x_{k|k-1}^i = f(x_{k-1}^i)$$

Compute the mean and covariance:

$$\hat{x}_{k|k-1} = \sum_{i=0}^{2n} \omega_m^i x_{k|k-1}^i$$

$$P_{xx,k} = \sum_{i=0}^{2n} \omega_c^i (x_{k|k-1}^i - \hat{x}_{k|k-1})(x_{k|k-1}^i - \hat{x}_{k|k-1})^T$$

- Measurement update:

Update sigma points through measurement function:

$$y_{k|k-1}^i = g(x_{k|k-1}^i)$$

Compute the mean and covariance:

$$\hat{y}_{k|k-1} = \sum_{i=0}^{2n} \omega_m^i y_{k|k-1}^i$$

$$P_{yy,k} = \sum_{i=0}^{2n} \omega_c^i (y_{k|k-1}^i - \hat{y}_{k|k-1})(y_{k|k-1}^i - \hat{y}_{k|k-1})^T$$

Compute the cross-covariance between the state and the measurement:

$$P_{xy,k} = \sum_{i=0}^{2n} \omega_c^i (x_{k|k-1}^i - \hat{x}_{k|k-1})(y_{k|k-1}^i - \hat{y}_{k|k-1})^T$$

- Calculate the Kalman gain and update the state estimation and covariance:

$$G_k = P_{xy,k} P_{yy,k}^{-1}$$

$$x_k = \hat{x}_{k|k-1} + G_k (y_k - \hat{y}_{k|k-1})$$

$$P_k = P_{xx,k} - G_k P_{yy,k} G_k^T$$

- end
-

5. VERIFICATION AND DISCUSSION

5.1 Construction of battery model and SOC estimation

According to the battery model introduced in Section 2, the battery parameter identification method introduced in Section 3, and the SOC estimation algorithm introduced in Section 4, the final simulation model is built in the MATLAB/Simulink environment. The overall framework of the improved ECM is shown in Figure 12. As a comparison, the battery model without current dependency but with temperature dependency and a model with neither with current dependency nor temperature dependency are also constructed. The battery parameters of the model that do not consider current are identified by a constant current rate (1/2C) at different temperatures, and the battery parameters of the model that only with SOC dependency are identified by a constant current rate (1/2C) at a fixed temperature (25°C).

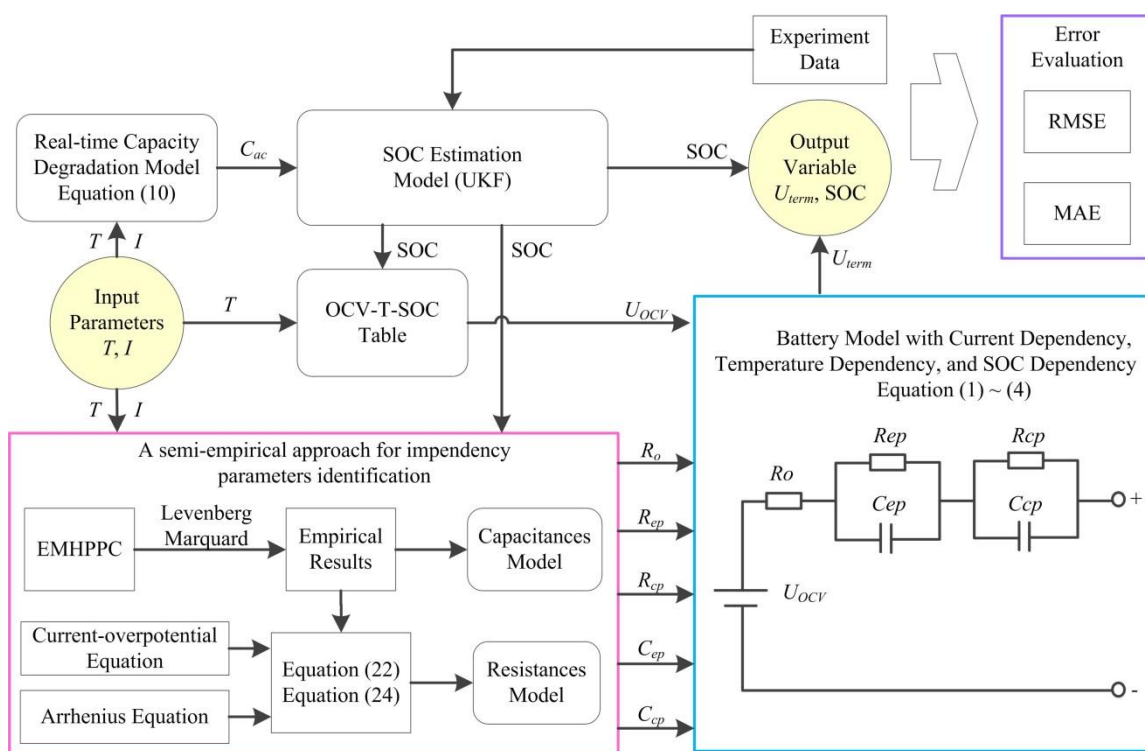


Figure 12. Schematic of the battery modeling and SOC estimation.

Unlike some previous research that used a constant discharge current to verify the accuracy of the model, we conducted a validation test in which the input current was generated by an EV under a dynamic situation. The New European Driving Cycle (NEDC) was employed to investigate the dynamic behavior of the test batteries. NEDC uses a 1180 s cycle to simulate the driving situation of EVs. It includes 780 s of urban road conditions and 400 s of suburban road conditions, and is based on a time-velocity profile. In the validation test, a scaled dynamic current sequence transferred from the time-velocity profile was applied to fit the specification of the test battery, as shown in Figure 13. The dynamic current validation tests were performed from 5°C to 45°C at an interval of 10°C.

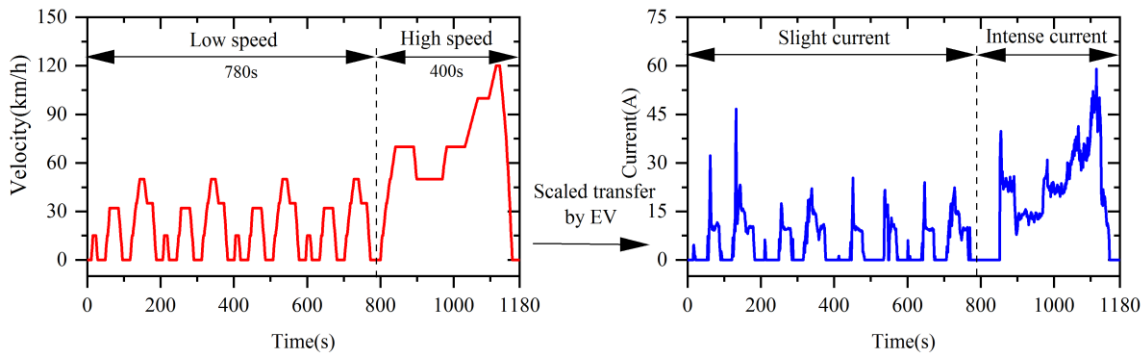


Figure 13. The framework of the NEDC validation test.

The verification tests include not only the verification of the improved battery model considering the dynamic current and temperature changes but also the SOC estimation. The mean absolute error (MAE) calculated by equation (31) and root mean square error (RMSE) calculated by equation (32) are employed to comprehensively evaluate the accuracy of our methods.

$$\text{MAE} = \frac{1}{t} \sum_{i=1}^t |U_{exp}(i) - U_{sim}(i)| \quad (33)$$

$$\text{RMSE} = \sqrt{\frac{1}{t} \sum_{i=1}^t [U_{exp}(i) - U_{sim}(i)]^2} \quad (34)$$

where U_{exp} denotes the experimental data, U_{sim} denotes the simulated data, and t denotes the time of the data point.

5.2. Results of the model verification

The voltage responses of the three battery models and errors at temperatures of 5°C, 15°C, 25°C, 35°C, and 45°C are shown in Figure 14. All of the simulated results of the three models have a tendency similar to that of the experimental data at different temperatures. The difference is that the errors between the simulated results of the three models and the experimental data. Figure 14 shows that among the three models, the simulation curve of the proposed model that with current dependency and temperature dependency has the best agreement with the experimental voltage profile and smallest errors at each temperature.

As shown in Figure 14, in the preceding part of the NEDC curve, the running speed of the EV is low, and the input test current is relatively small and stable. At this time, the impact of current on modeling accuracy can be ignored, so the simulated results between the models with current dependency and without current dependency are similar. However, as the speed of electric vehicles increases, the battery current begins to increase rapidly and change drastically in the final stage of the NEDC. At this moment, the current plays a crucial role in ensuring the modeling accuracy, so the simulated voltage of the battery model, which considers the influence of the current, will be closer to the experimental data. Meanwhile, in the high current range, the response voltage U_{CH} of the model with current dependency is higher than the response voltage U_{TH} of the model without current

dependency resulting from by the lower battery resistance R_{CH} . This is consistent with our work introduced in Section 3, showing that the internal resistance of the battery decreases with increasing current.

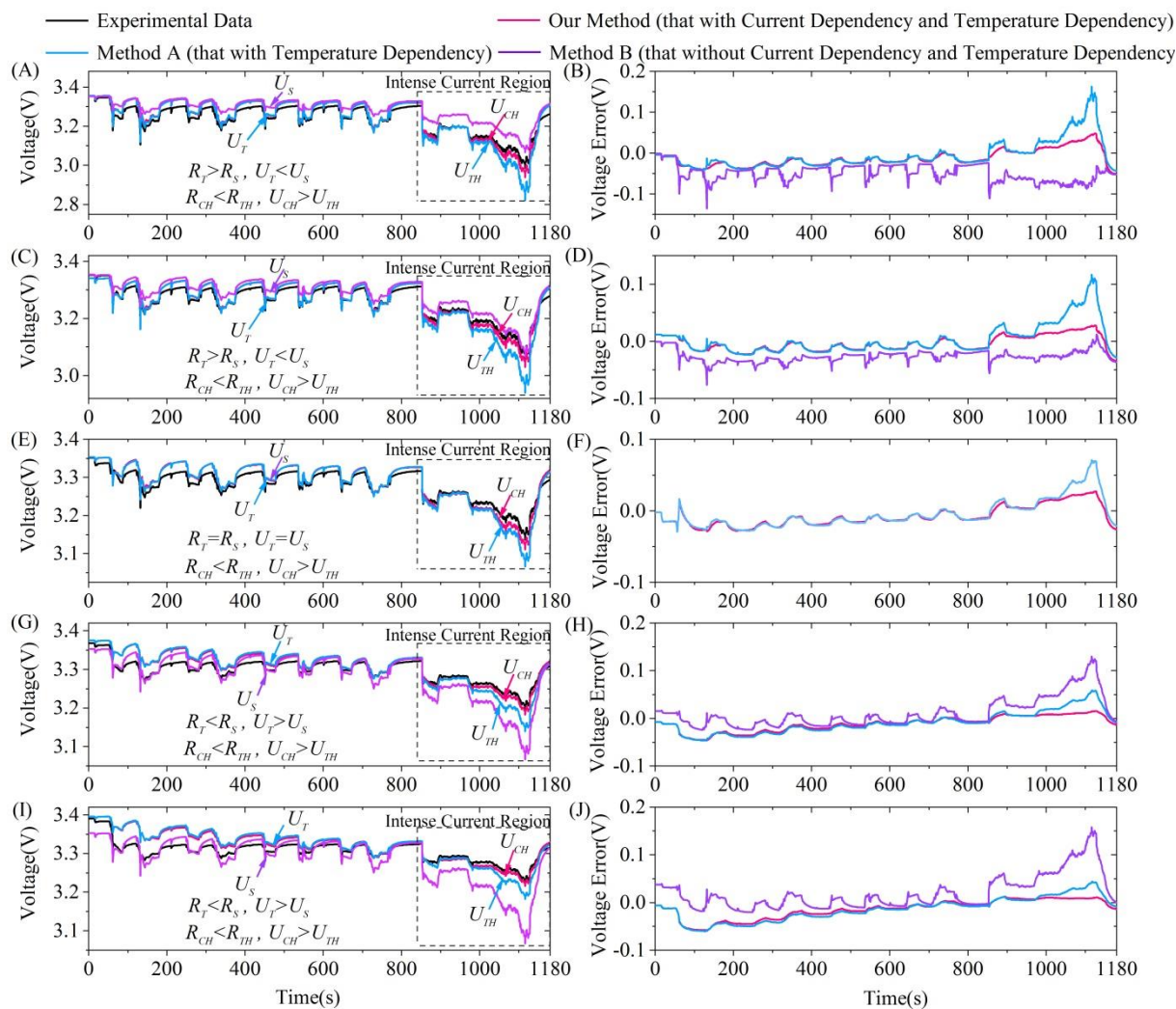


Figure 14. The verification results and errors at 5°C (A), (B); 15°C (C), (D); 25°C(E), (F); 35°C(G), (H); 45°C(I), (J).

Temperature is another crucial factor affecting modeling accuracy. As shown in Figure 15, the battery model with temperature dependency has a smaller error in each test temperature than the battery model that does not consider temperature. According to the Arrhenius equation introduced in Section 3, the battery internal resistance decreases with the increasing temperature, so the battery internal resistance R_T at 5°C and 15°C is higher than the resistance R_C at 25°C, and the battery internal resistance R_T at 35°C and 45°C is lower than R_C at 25°C. We can obtain from the simulation results that when the temperature is lower than 25°C, the simulation voltage U_T considering the temperature is lower than the simulation voltage U_C without considering the temperature. In contrast, when the temperature is lower than 25°C, the simulation voltage U_T considering the temperature is higher than

U_C without considering the temperature. This is powerful support for the Arrhenius equation from the side of the battery voltage response.

The MAE and RMSE during the entire NEDC of the three models depicted in Table 3 indicate that the model with current dependency parameters can perform better than the other models in responding to the dynamic behavior. The RMSE and MAE during the intense current region of the three models shown in Table 4 confirm that when the current is high and intensively changes, the current has been an essential factor affecting battery performance and cannot be ignored. It can be observed that even at low temperatures with a large current output, the accuracy of the simulated results can be improved significantly by the model complemented by current dependency parameters.

The simulated results and error analysis mentioned above show that the proposed model with current dependency and temperature dependency is sufficiently accurate and suitable to track the dynamic behavior of the battery under complex driving conditions.

Table 3. MAEs and RMSEs of modeling verification during the entire NEDC process.

| Entire NEDC | 5°C | | 15°C | | 25°C | | 35°C | | 45°C | |
|-------------|--------|--------|--------|--------|--------|--------|--------|--------|--------|--------|
| | MAE | RMSE |
| Our method | 0.0206 | 0.0236 | 0.0121 | 0.0137 | 0.014 | 0.0158 | 0.0157 | 0.0195 | 0.0185 | 0.0243 |
| Method A | 0.0264 | 0.0345 | 0.0182 | 0.0262 | 0.0163 | 0.0201 | 0.0204 | 0.0245 | 0.0227 | 0.0282 |
| Method B | 0.0492 | 0.0530 | 0.0262 | 0.0279 | 0.0163 | 0.0201 | 0.0213 | 0.0323 | 0.0265 | 0.0406 |

Table 4. MAEs and RMSEs of modeling verification during the intense current region.

| Intense current | 5°C | | 15°C | | 25°C | | 35°C | | 45°C | |
|-----------------|--------|--------|--------|--------|--------|--------|--------|--------|--------|--------|
| | MAE | RMSE |
| Our method | 0.0188 | 0.0232 | 0.0145 | 0.0161 | 0.013 | 0.0148 | 0.008 | 0.0085 | 0.0076 | 0.0081 |
| Method A | 0.0365 | 0.0502 | 0.0323 | 0.0415 | 0.0198 | 0.0255 | 0.0183 | 0.0235 | 0.0143 | 0.018 |
| Method B | 0.0595 | 0.0622 | 0.023 | 0.0244 | 0.0198 | 0.0255 | 0.0421 | 0.0528 | 0.0532 | 0.0663 |

5.3. Results of the SOC estimation verification

The accuracy of SOC estimation is subject to the employed algorithm and battery model. There is an abundance of literature focus on the SOC estimation algorithm, and powerful evidence shows that the model-based SOC estimation method, especially KF family algorithms, is more suitable for electric vehicle applications due to the low computational load, high accuracy, and good noise filtering performance [42]. The core work of this paper is to propose the RCDM and establish a battery model with current and temperature dependence to improve the accuracy of SOC estimation, rather than developing a novel algorithm tool. Therefore, the UKF algorithm is selected for SOC estimation from the various existing algorithms. The effect of capacity degradation, dynamic currents and temperatures on SOC estimation will be discussed in the following sections. To observe the method accuracy in a wide range of SOCs, the test process was composed of four continuous NEDCs. An incorrect SOC

with an offset of 10% was used for the initial values of all three methods, and the reference SOC was obtained by the Ampere-hour integral method.

5.3.1. Effect of capacity degradation on SOC estimation

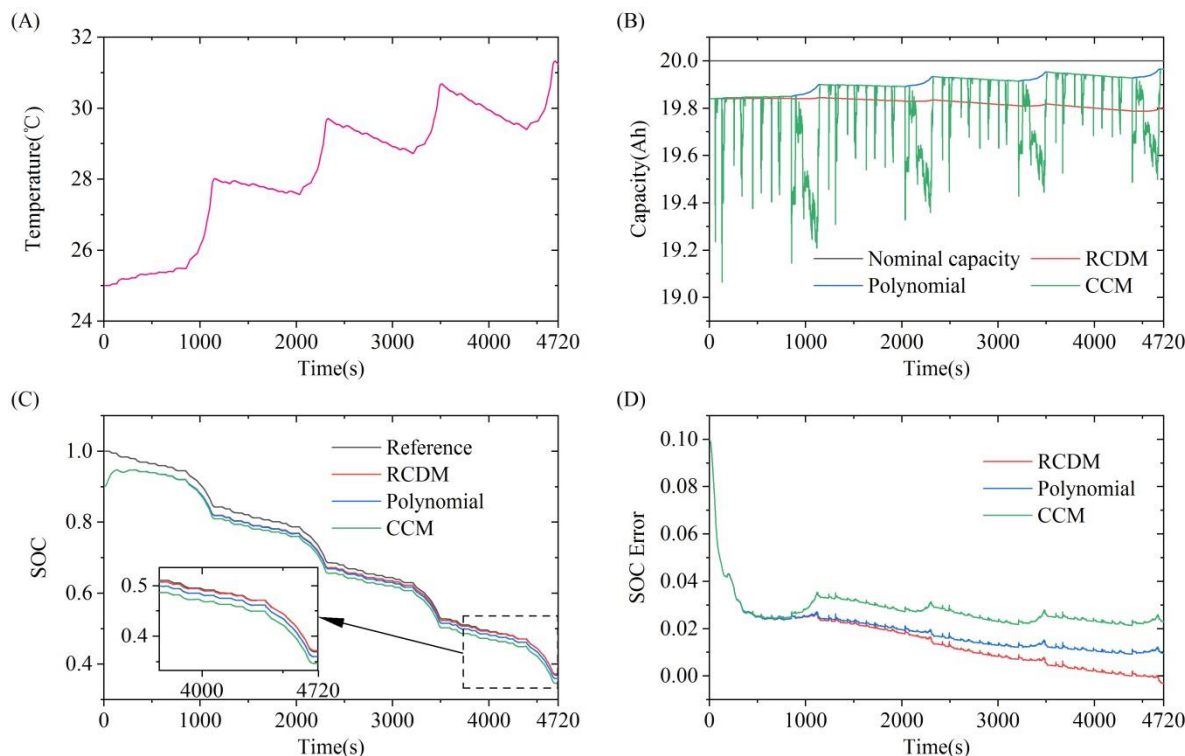


Figure 15. Verification results at 5°C: temperature of battery (A), capacity estimation results (B), SOC verification results (C) and errors (D) employing different capacity models.

To investigate the effect of the capacity on SOC estimation, the verification tests are performed by employing the battery model introduced in section 2.1 and combined with three different capacity models including the proposed RCDM, polynomial [13, 20], and capacity correction model (CCM) [9]. The polynomial model ignores the current effect on capacity and employs the equation (5) to express the capacity change under dynamic currents and temperatures. The CCM uses correction factors to reflect the degradation of maximum release capacity. And the reference capacity is the nominal capacity.

The temperature of the tested battery during the verification process is shown in Figure 15(A). In the first NEDC, the battery temperature rises with the increasing loading current, however, in the remaining three NEDCs, the battery temperature only rises in the intense current region. When the speed of EV is low, the battery heat dissipation rate is greater than the heating rate, causing the temperature to drop. The capacity and SOC estimation results are shown in Figure (B), (C), (D). The polynomial model can well track the temperature effect on capacity and the estimation results change as the battery temperature fluctuations. However, the actual capacity is also influenced by the current which the polynomial model does not reflect. Therefore, the SOC estimation error employing the

polynomial capacity model will increase in each intense current region. The CCM employs the temperature and current correction factors to estimate the actual capacity, however, current changes significantly in the entire tested produce which resulting the current correction factor is also not a constant. The fluctuated capacity estimation results will be distorted, leading to the increased error of the final SOC estimation result as shown in Figure (C) and (D). Compared with the polynomial and CCM, the proposed RCDM performs much better on SOC estimation. The capacity obtained by the RCDM will not only increase with the temperature rise but also decrease with the increasing discharge current rate. In the entire verification produce, the RCDM can well express the actual capacity under dynamic currents and temperatures. The MAEs and RMSEs of SOC estimation results using different methods are tabulated in Table 5. Although both the SOC estimation errors using different capacity models are small, but overall, the proposed RCDM can provide more accurate and stable SOC estimation results.

Table 5. MAEs and RMSEs of SOC verification employing different capacity models.

| Capacity model | MAE | RMSE |
|----------------|--------|--------|
| RCDM | 0.0047 | 0.0054 |
| Polynomial | 0.0073 | 0.0085 |
| CCM | 0.018 | 0.0219 |

5.3.2. Effect of current and temperature on SOC estimation

To investigate the effect of current and temperature on SOC estimation, the verification testes are performed not only by employing the proposed method, but also the common method A [56, 65] that considered the temperature influence and common method B [66] that considered neither the current nor the temperature influence are used for comparison.

It can be seen from Figure 16 that all three methods will quickly improve the error caused by the initial incorrect value after a short period and closely approach the reference SOC. However, our method and method A have basically the same error response time, which is much less than that of method B. Moreover, the SOC curve obtained by our method can track the reference SOC better than those obtained by the other two methods in all the test processes at different temperatures. Especially in the four intense-current regions, the error of our method did not fluctuate significantly with drastic changes in the current and remained at a low level, similar to other regions. As a comparison, both the errors of method A and method B increase significantly. At the same time, we have also observed that the maximum error of common method A in the intense current regions decreased gradually over time, that is, $\delta_{T,4} < \delta_{T,3} < \delta_{T,2} < \delta_{T,1}$. This is because the UKF algorithm can improve the accumulation of errors as the number of iterations increases, which also confirms the effectiveness of the UKF in estimating battery SOC estimation. A similar trend was found in method B, but the maximum error of method B in the four intense current regions does not strictly decrease with the increase in the number of iterations due to the temperature factor.

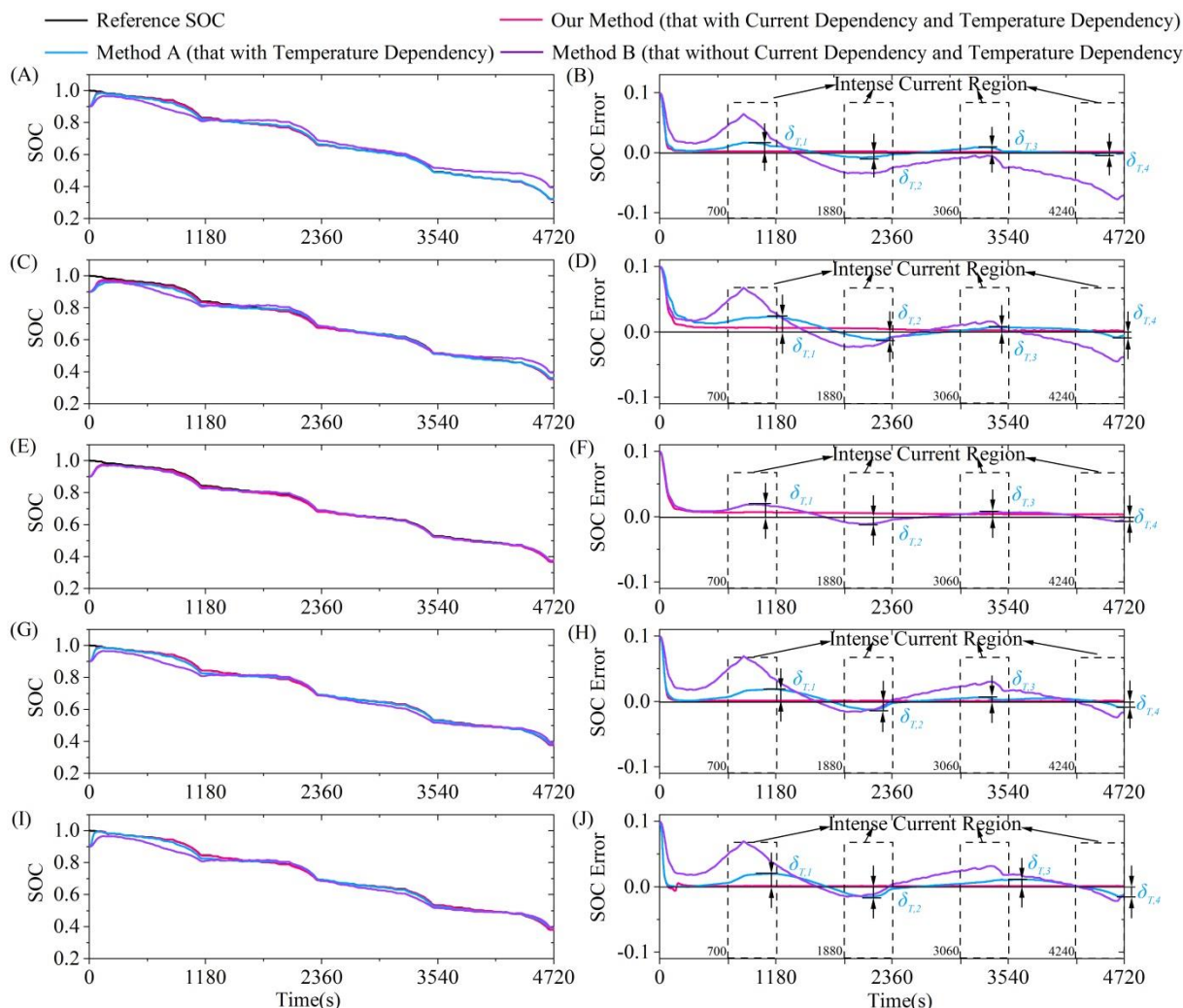


Figure 16. The SOC verification results and errors at 5°C (A), (B); 15°C (C), (D); 25°C(E), (F); 35°C(G), (H); 45°C(I), (J).

Table 6. MAEs and RMSEs of SOC verification during the intense current region.

| Intense current | 5°C | | 15°C | | 25°C | | 35°C | | 45°C | |
|-----------------|--------|--------|--------|--------|--------|--------|--------|-------|--------|--------|
| | MAE | RMSE | MAE | RMSE | MAE | RMSE | MAE | RMSE | MAE | RMSE |
| Our method | 0.0017 | 0.0017 | 0.0038 | 0.0042 | 0.0049 | 0.0051 | 0.001 | 0.001 | 0.0009 | 0.0009 |
| Method A | 0.0072 | 0.0087 | 0.0097 | 0.0121 | 0.0089 | 0.0103 | 0.0083 | 0.01 | 0.0106 | 0.0119 |
| Method B | 0.038 | 0.0434 | 0.0287 | 0.0333 | 0.0089 | 0.0103 | 0.026 | 0.032 | 0.0258 | 0.0321 |

Table 6 shows the MAE and RMSE of the three methods in the intense current regions. Our method has the smallest error at each test temperature. Compared to method A, the values of MAE and RMSE for SOC estimation with the proposed battery model are reduced by 76.4% and 80.4%, 60.8% and 65.3%, 44.9% and 50.5%, 87.9% and 90%, 91.5% and 92.4%, respectively. Compared to method B, the values of MAE and RMSE for SOC estimation with our method are reduced by 95.5% and 96.1%, 86.8% and 87.4%, 44.9% and 50.5%, 96.2% and 96.9%, 96.5% and 97.2%, respectively. This

indicates that our method with both current dependency and temperature dependency, and integrating the UKF, can achieve higher accuracy in SOC estimation.

6. CONCLUSION

The current and temperature are critical factors that affect battery performance, and it is necessary to consider them when battery modeling and SOC estimation are performed. An improved ECM with current dependency and temperature dependency combined with a RCDM and semi-empirical parameter identification method is proposed to more accurately reflect the non-linear response of batteries under dynamic currents and various temperatures. The battery internal resistance exhibits a decreasing trend as the current increases or temperature decreases. The current and temperature dependency of the capacity and impedance parameters should not be ignored. Excellent agreements are obtained between the simulation results elicited by our model and experimental data in all the dynamic verification tests conducted over a wide range of temperatures. This proves that the proposed model can improve the accuracy of battery modeling compared with the common models that do not consider current. Subsequently, the proposed model, in conjunction with the UKF algorithm, was used for SOC estimation verification. The results show that the proposed model can better track the SOC in the intense current region. In this paper, we not only consider the impact of temperature and SOC on battery performance, as have other scholars, but also investigate the influence of current. Verification results show that under the complex driving conditions of EVs, higher modeling, and SOC estimation accuracy can be achieved when considering current.

ACKNOWLEDGMENTS

This research was supported by the National Key Research and Development Project of China (Grant No. 2018YFB0106204-03).

References

1. M. Shen and Q. Gao, *Int. J. Energy Res.*, 43 (2019) 5042.
2. W. Shuai, E. Li and H. Wang, *Int. J. Energy Res.*, 44 (2020) 8372.
3. X. Lai, L. He, S. Wang, L. Zhou, Y. Zhang, T. Sun and Y. Zheng, *J. Cleaner Prod.*, 255 (2020) 120203.
4. F. Yang, D. Wang, Y. Zhao, K. Tsui and S. J. Bae, *Energy*, 145 (2018) 486.
5. C. Wu, R. Fu, Z. Xu and Y. Chen, *Energies*, 10 (2017) 1486.
6. N. Tian, Y. Wang, J. Chen and H. Fang, *J. Energy Storage*, 29 (2020) 101282.
7. H. He, X. Zhang, R. Xiong, Y. Xu and H. Guo, *Energy*, 39 (2012) 310.
8. X. Liu, J. Wu, C. Zhang and Z. Chen, *J. Power Sources*, 270 (2014) 151.
9. Y. Wang, C. Zhang and Z. Chen, *J. Power Sources*, 279 (2015) 306.
10. V. Duong, H. A. Bastawrous, K. Lim, K. W. See, P. Zhang and S. X. Dou, *J. Power Sources*, 296 (2015) 215.
11. C. Campestrini, T. Heil, S. Kosch and A. Jossen, *J. Energy Storage*, 8 (2016) 142.
12. S. Ma, M. Jiang, P. Tao, C. Song, J. Wu, J. Wang, T. Deng and W. Shang, *Prog. Nat. Sci-*

- mater.*, 28 (2018) 653.
13. H. Pang, L. Guo, L. Wu and X. Jin, *Int. J. Energy Res.*, 44 (2020) 7254.
 14. C. S. Chin, Z. Gao, J. H. K. Chiew and C. Zhang, *Energies*, 11 (2018) 2467.
 15. X. Liu, Y. He, G. Zeng, J. Zhang and X. Zheng, *Energy Technol.*, 6 (2018) 1352.
 16. H. Cho, W. Choi, J. Go, S. Bae and H. Shin, *J. Power Sources*, 198 (2012) 273.
 17. I. Bloom, B. W. Cole, J. J. Sohn, S. A. Jones, E. G. Polzin, V. S. Battaglia, G. L. Henriksen, C. Motloch, R. Richardson, T. Unkelhaeuser, D. Ingersoll, H. L. Case and A. I. U. S. Argonne National Lab. ANL, *J. Power Sources*, 101 (2001) 238.
 18. J. Wang, P. Liu, J. Hicks-Garner, E. Sherman, S. Soukiazian, M. Verbrugge, H. Tataria, J. Musser and P. Finamore, *J. Power Sources*, 196 (2011) 3942.
 19. F. Feng, R. Lu and C. Zhu, *Energies*, 7 (2014) 3004.
 20. F. Guo, G. Hu, P. Zhou, J. Hu and Y. Sai, *Int. J. Energy Res.*, 44 (2020) 7357.
 21. W. Waag, S. Kaebitz and D. U. Sauer, *Appl. Energy*, 102 (2013) 885.
 22. J. Zhu, Z. Sun, X. Wei and H. Dai, *J. Appl. Electrochem.*, 46 (2016) 157.
 23. W. Waag, C. Fleischer and D. U. Sauer, *J. Power Sources*, 242 (2013) 548.
 24. W. Waag, C. Fleischer and D. U. Sauer, *J. Power Sources*, 237 (2013) 260.
 25. B. V. Ratnakumar, M. C. Smart, L. D. Whitcanack and R. C. Ewell, *J. Power Sources*, 159 (2006) 1428.
 26. D. A. Noren and M. A. Hoffman, *J. Power Sources*, 152 (2005) 175.
 27. C. Fleischer, W. Waag, H. Heyn and D. U. Sauer, *J. Power Sources*, 262 (2014) 457.
 28. J. Zhu, M. Knapp, M. S. D. Darma, Q. Fang, X. Wang, H. Dai, X. Wei and H. Ehrenberg, *Appl. Energy*, 248 (2019) 149.
 29. Y. Song, D. Liu, H. Liao and Y. Peng, *Appl. Energy*, 261 (2020) 114408.
 30. F. Yang, W. Li, C. Li and Q. Miao, *Energy*, 175 (2019) 66.
 31. J. Meng, G. Luo and F. Gao, *IEEE Trans. Power Electron.*, 31 (2016) 2226.
 32. J. Lu, Z. Chen, Y. Yang and M. L. V., *IEEE Access*, 6 (2018) 20868.
 33. D. E. Acuña and M. E. Orchard, *Mech. Syst. Sig. Process.*, 85 (2017) 827.
 34. M. Ye, H. Guo and B. Cao, *Appl. Energy*, 190 (2017) 740.
 35. L. Zhao, Z. Liu and G. Ji, *Control Eng. Pract.*, 81 (2018) 114.
 36. C. Lin, H. Mu, R. Xiong and W. Shen, *Appl. Energy*, 166 (2016) 76.
 37. C. Chen, R. Xiong and W. Shen, *IEEE Trans. Power Electron.*, 33 (2018) 332.
 38. Y. Shen, *Electrochim. Acta*, 283 (2018) 1432.
 39. F. Guo, G. Hu, S. Xiang, P. Zhou, R. Hong and N. Xiong, *Energy*, 178 (2019) 79.
 40. Y. Xu, M. Hu, A. Zhou, Y. Li, S. Li, C. Fu and C. Gong, *Appl. Math. Modell.*, 77 (2020) 1255.
 41. C. Chen, R. Xiong, R. Yang, W. Shen and F. Sun, *J. Cleaner Prod.*, 234 (2019) 1153.
 42. P. Shrivastava, T. K. Soon, M. Y. I. B. Idris and S. Mekhilef, *Renewable Sustainable Energy Rev.*, 113 (2019) 109233.
 43. F. Yan, C. Zhang, C. Du and C. Cheng, *Int. J. Electrochem. Sci.*, 13 (2018) 12360.
 44. Y. Guo, Z. Zhao and L. Huang, *Energy Procedia*, 105 (2017) 4146.
 45. Q. Ouyang, R. Ma, Z. Wu, G. Xu and Z. Wang, *Energies*, 13 (2020) 4968.
 46. J. Peng, J. Luo, H. He and B. Lu, *Appl. Energy*, 253 (2019) 113520.
 47. B. Jiang, H. Dai, X. Wei and T. Xu, *Appl. Energy*, 253 (2019) 113619.
 48. L. Chen, R. Xu, W. Rao, H. Li, Y. Wang, T. Yang and H. Jiang, *Int. J. Electrochem. Sci.*, 14 (2019) 4124.
 49. H. He, R. Xiong and J. Fan, *Energies*, 4 (2011) 582.
 50. M. Farag, H. Sweity, M. Fleckenstein and S. Habibi, *J. Power Sources*, 360 (2017) 618.
 51. J. Marcicki, M. Canova, A. T. Conlisk and G. Rizzoni, *J. Power Sources*, 237 (2013) 310.
 52. X. Dang, L. Yan, K. Xu, X. Wu, H. Jiang and H. Sun, *Electrochim. Acta*, 188 (2016) 356.
 53. E. Chemali, P. J. Kollmeyer, M. Preindl and A. Emadi, *J. Power Sources*, 400 (2018) 242.
 54. A. Barai, W. D. Widanage, J. Marco, A. McGordon and P. Jennings, *J. Power Sources*, 295

- (2015) 99.
55. X. Lai, Y. Zheng and T. Sun, *Electrochim. Acta*, 259 (2018) 566.
 56. X. Liu, Z. Chen, C. Zhang and J. Wu, *Appl. Energy*, 123 (2014) 263.
 57. T. R. Ashwin, Y. M. Chung and J. Wang, *J. Power Sources*, 328 (2016) 586.
 58. N. Sharma, D. H. Yu, Y. Zhu, Y. Wu and V. K. Peterson, *J. Power Sources*, 342 (2017) 562.
 59. M. Doyle, J. P. Meyers, J. Newman and W. D. U. DuPont Central Research And Development, *J. Electrochem. Soc.*, 147 (2000) 99.
 60. W. Xu, J. Xu and X. Yan, *J. Power Electron.*, 20 (2020) 292.
 61. F. Feng, S. Teng, K. Liu, J. Xie, Y. Xie, B. Liu and K. Li, *J. Power Sources*, 455 (2020) 227935.
 62. Y. Tian, B. Xia, W. Sun, Z. Xu and W. Zheng, *J. Power Sources*, 270 (2014) 619.
 63. W. Zhang, W. Shi and Z. Ma, *J. Power Sources*, 289 (2015) 50.
 64. J. Zhang and C. Xia, *Int. J. Electr. Power Energy Syst.*, 33 (2011) 472.
 65. X. Ding, D. Zhang, J. Cheng, B. Wang and P. C. K. Luk, *Appl. Energy*, 254 (2019) 113615.
 66. M. García-Plaza, D. Serrano-Jiménez, J. Eloy-García Carrasco and J. Alonso-Martínez, *J. Power Sources*, 275 (2015) 595.

© 2021 The Authors. Published by ESG (www.electrochemsci.org). This article is an open access article distributed under the terms and conditions of the Creative Commons Attribution license (<http://creativecommons.org/licenses/by/4.0/>).